

# Simulations of Stellar Collisions Involving Pre-Main Sequence Stars

Daniel Laycock & Alison Sills

*Department of Physics and Astronomy, McMaster University, 1280 Main Street West,  
Hamilton, Ontario, L8S 4M1, Canada*

`laycockdt@mcmaster.ca, asills@mcmaster.ca`

## ABSTRACT

In this paper, we present the results of smoothed particle hydrodynamic (SPH) simulations of collisions between pre-main sequence stars and a variety of other kinds of stars. Simulations over a range of impact parameters and velocities were performed. We find that pre-main sequence stars tend to “wrap themselves” around their impactor. We discuss the probable evolutionary state of products of collisions between pre-main sequence stars and pre-main sequence, main sequence, giant branch, and compact stars. The nature of the collision product does not depend strongly on the impact parameter or the velocity of the collision.

*Subject headings:* hydrodynamics – stars:pre-main sequence

## 1. Introduction

Over the past decade, dynamical models of stellar clusters have become much more realistic. This realism takes the form of an increasingly complicated treatment of the individual stars in the cluster. For years, simple dynamical models only considered stars as single equal-mass, non-evolving points (e.g. Cohn 1980). The introduction of a mass function into dynamical models quickly necessitated some treatment of stellar evolution, since high mass stars have much shorter lifetimes than low mass stars. Mass loss from high mass stars can also have a substantial impact on the dynamical evolution of the cluster (Elson, Hut, & Inagaki 1987). Binary stars also have a substantial impact on the cluster, by acting as energy sources or sinks. Before globular clusters were thought to have primordial binaries, dynamically produced binaries were recognized as a key population for halting core collapse (Hut et al. 1992). Clusters also have primordial binaries, and those binary systems can affect the cluster evolution from its birth.

Stellar dynamicists also realized that the point mass approximation for stars was neglecting a number of dynamically significant processes in clusters. Allowing stars to have radii, and having those radii change with the evolution of the star, was an important next addition to stellar dynamics simulations (Hut & Inagaki 1985; Aarseth 1996; Portegies Zwart et al. 2001; Hurley et al. 2001). Finite stellar radii are most important for two aspects of these simulations. First, binary stars can undergo mass transfer as one member of the system fills its Roche lobe, either through evolution of the star or dynamical modification of the orbital parameters of the system. Altering the parameters of binary systems will change how the binaries affect the evolution of the cluster. In the extreme case, the two components of the binary system can merge. Secondly, stars with finite radii can collide with other stars. The low velocity stellar collisions that occur in star clusters produce blue stragglers (Sills et al. 1997) and could produce other non-standard stellar populations. These populations in turn can change the local dynamical evolution in the cluster.

Until recently, all work on cluster modelling assumed that all stars began their lives on the main sequence. However, low mass stars make up the bulk of stars in a cluster for any reasonable initial mass function. Low mass stars also have significant pre-main sequence lifetimes. For some young open clusters, most of the stars are still on the pre-main sequence. These young stars have radii which can be up to  $\sim 10$  times larger than their main sequence radii (Siess, Dufour & Forestini 2000). Therefore, some binaries could have undergone an episode of mass transfer that is not taken into account. Also, larger stars are more likely to have experienced a collision; those collision products will have been missed in previous simulations. Dynamical simulations which include a pre-main sequence phase show that there can be notable effects on the overall cluster evolution (Wiersma, Sills & Portegies Zwart, in preparation). However, in order to properly include the pre-main sequence phase in stellar dynamics calculations, we need to understand collisions with pre-main sequence stars, and the properties of the collision products. Currently no such calculations are available in the literature.

In this paper, we present smoothed particle hydrodynamic (SPH) simulations of direct collisions between pre-main sequence stars and a variety of other stellar populations (main sequence, giant branch, compact objects). We study collisions at a variety of impact parameters and velocities, and determine the structure and likely evolution of the collision products. In section 2, we outline our simulation method and initial conditions. We present the results in section 3, and discuss their implications for stellar dynamics in section 4.

## 2. Method

The collisions studied in this paper were simulated using the smooth particle hydrodynamics (SPH) method (Benz 1990; Monaghan 1992), where the SPH particles represent the stellar gas. The three dimensional code we used is described in detail in Sills et al. (2002), and is the parallel version of the code described in Bate, Bonnell & Price (1995). It uses a tree to solve for the gravitational forces and to find the nearest neighbours (Benz 1990). We use the standard form of artificial viscosity with  $\alpha = 1$  and  $\beta = 2.5$  (Monaghan 1992), and an adiabatic equation of state. The thermodynamic quantities are evolved by following the change in internal energy. Both the smoothing length and the numbers of neighbours can change in time and space. The smoothing length is varied to keep the number of neighbours approximately constant ( $\sim 50$ ).

Collisions involving five different types of stars were examined in this paper. Specifically, we simulated interactions between pre-main sequence (PMS) stars and white dwarfs (WD), giant branch (GB), zero age main sequence (ZAMS), turnoff main sequence (TAMS), and other pre-main sequence stars. The density and composition profiles of the stellar models were calculated using the Yale Rotational Evolution Code (YREC, Guenther et al. (1992)). The stars were composed of  $\sim 10,000$  SPH particles except for the giant which required  $\sim 50,000$  particles in order to properly model its steeper density gradient. The giant also contained a point mass core to model the very high density in this region. The white dwarf was modeled as a point mass due to its very small radius and large density compared to the other stars studied. The SPH particles were equally spaced throughout the star, and their masses were varied to produce the required density profile. The stars were all run alone in the SPH code in order to allow them to relax before being collided. Figure 1 shows the density profile of the SPH particles for the pre-main sequence star used in all collisions, as well as the YREC model (dashed line). This pre-main sequence star is barely off the deuterium-burning birthline, and has an age of  $\sim 100,000$  years. Pre-main sequence stars actually spend little time in this part of the HR diagram. Our  $0.8 M_{\odot}$  model spends 70 Myr contracting to the main sequence, and only the first 10 Myr of that time is on the Hayashi track. The rest of the time is spent traveling horizontally across the HR diagram. The structure of the pre-main sequence star during this horizontal phase is very similar to that of a main sequence star. Therefore, in order to expand our understanding of stellar collision products with very different properties, we chose an extremely young PMS star for our collision simulations.

Table 1 gives the parameters of all the parent stars studied in this paper. The number of SPH particles used in each model is given in units of 1,000 particles. All stars are  $0.8 M_{\odot}$ , except the white dwarf which is  $0.6 M_{\odot}$ . The stars have solar metallicity,  $Z=0.0188$ , and an initial helium abundance of  $Y=0.27$ . The giant branch star was evolved to about halfway up

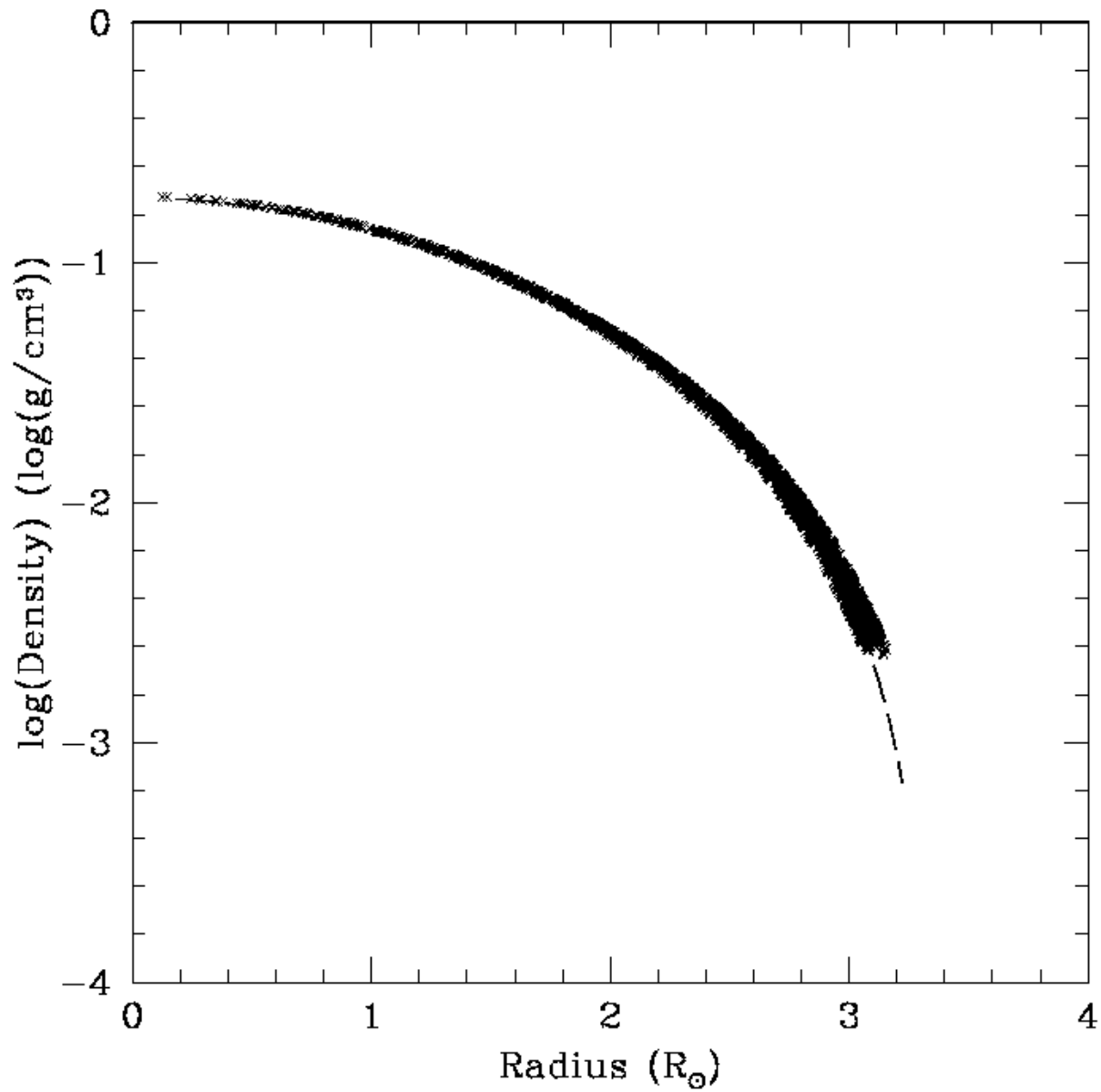


Fig. 1.— Logarithm of the density versus radius for the pre-main sequence star used in all simulations. The dashed line is the stellar model from YREC while the x's are the SPH representation of this star.

the giant branch. This giant was chosen as a representative average giant that might collide with another object – the cross section for collision increases as the giant’s radius increases, but its lifetime at that radius decreases.

It is, of course, unreasonable to expect stars of the same mass to be simultaneously on the pre-main sequence and on the giant branch in the same cluster. However, in this paper we are interested in the gross properties of collisions involving pre-main sequence stars. At that level, the results of collisions between stars of different masses can be extrapolated from the results presented here.

The helium composition profile for the terminal age main sequence (TAMS) star is displayed in figure 2. The helium composition profiles of the pre-main sequence, zero age main sequence, and giant branch stars are flat. This is true for the GB because all of the helium enriched fluid is within the point mass core, so the SPH particles in the rest of the star all have essentially the same content.

In this paper, we consider all five of the stars as impactors to the pre-main sequence star. The frame of reference used for simulations was such that the stars’ center of mass initially resided at the origin. An initial separation of  $30 R_{\odot}$  was used to ensure that in all initial setups the stars were separated by at least 4 times the radius of the larger star. This allowed tidal effects to be ignored in the original alignment. The stars were set up on a zero-energy orbit initially under the assumption that the stars were point masses. The relative velocities at infinity of the stars ranged from 10km/s to 100km/s, spanning the range of typical velocities found in collisions in clusters. The lower bound, 10 km/s, is the typical velocity dispersion in globular clusters. The upper bound, 100 km/s, is a representative upper bound on the velocity a binary system could provide in a resonance encounter which resulted in a physical collisions. The velocity dispersion in open clusters is smaller than our lower bound (typically a few km/s). For collisions with low velocities at infinity, the actual impact speed is dominated by the escape velocity at the surface of the two stars. We expect our results for 10 km/s to be a reasonable approximation to all low velocity collisions. Initially, the stars were nonrotating, so any angular momentum after the collision was purely a result of the initial orbit. The orbital plane was chosen to be the  $z=0$  plane.

The impact parameter  $r_p$  was varied from 0, for a head-on collision, to 1 (in units of  $R_1 + R_2$ , the radii of the two stars), for a grazing collision, in order to gain an understanding of the results for collisions ranging over the whole radius of the star. Collisions with an impact parameter greater than 1 could result in a merged daughter star, due to the fact that tides are raised on the stars as they approach each other, dissipating energy and possibly causing contact as they pass. This case was not considered, however, due to its much larger computational requirements. If the first pass of the stars does not dissipate enough energy

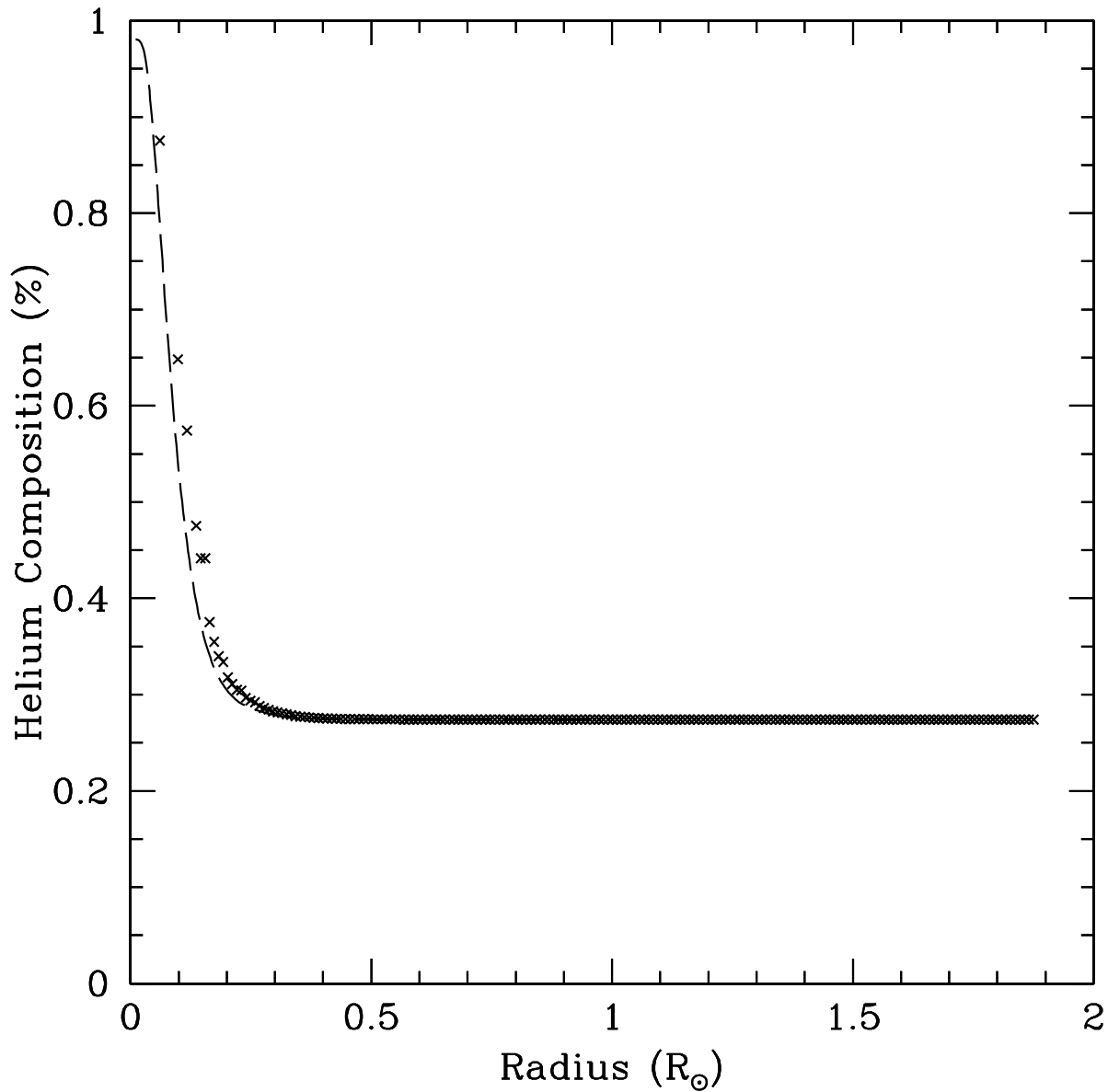


Fig. 2.— Helium composition as a function of radius for the TAMS star used in simulations. The dashed line is the stellar model from YREC and the x's are the SPH representation of this star.

then the stars will take a substantial amount of time to merge because they can convert more kinetic energy back into potential energy and therefore achieve larger separations. Obviously, if the impact parameter is larger than the combined radius then very little energy will be dissipated on the first pass. Also, some impactors were not considered at an impact parameter of 1 if their companions at an impact parameter of 0.5 took a long time to merge, also due to the large computational requirements.

### 3. Results

Table 2 summarizes the results of the simulations performed. In column 1, we give a letter which names each run. Column 2 indicates the impactor of the PMS star used for the run. Column 3 gives the impact parameter, in units of the total radii of the two stars, while column 4 gives the initial velocity at infinity of the pair. The remaining data provides information about the daughter star produced. Column 5 indicates if the stars merged before the simulation was ended. Columns 6-8 display the daughter stars' masses in units of  $M_{\odot}$ , final angular momentum around the z-axis in units of  $g \text{ cm}^2 \text{s}^{-1}$ , and the ratio of rotational kinetic energy to absolute potential energy respectively. The final column indicates the percent change in total energy throughout the course of the simulation.

#### 3.1. Numerical Resolution

Case AC, a head-on collision between a pre-main sequence star and a white dwarf, was run with three pre-main sequence stars of varying number of particles to test the effects of resolution on the results we obtained. Along with the 10 000 particle case described in the previous section, two additional higher resolutions, 50 000 and 100 000 particles, were run. Figure 3 shows a plot of the final density profiles for these three runs. The solid line shows the 10 000 particle case, the long dashed line is the result of the 50 000 particle case, and the dotted line is the result of the 100 000 particle case. This plot shows that the resolution of the pre-main sequence star did not significantly alter the final product, especially in the central region of the daughter star. There are no noticeable differences in the inner 70% by mass of these three density profiles. Slight disagreement is visible in the outer regions of the star. However, this region is the least settled and will be subject to further relaxation. The density profile of the lowest resolution at future times shows that the outer region of the star is indeed slowly decreasing in density as the star continues to relax, while the density at the core is not changing at all. This, as can be seen in the plot, would bring it into closer agreement with the other resolutions. It is important to note that although there are

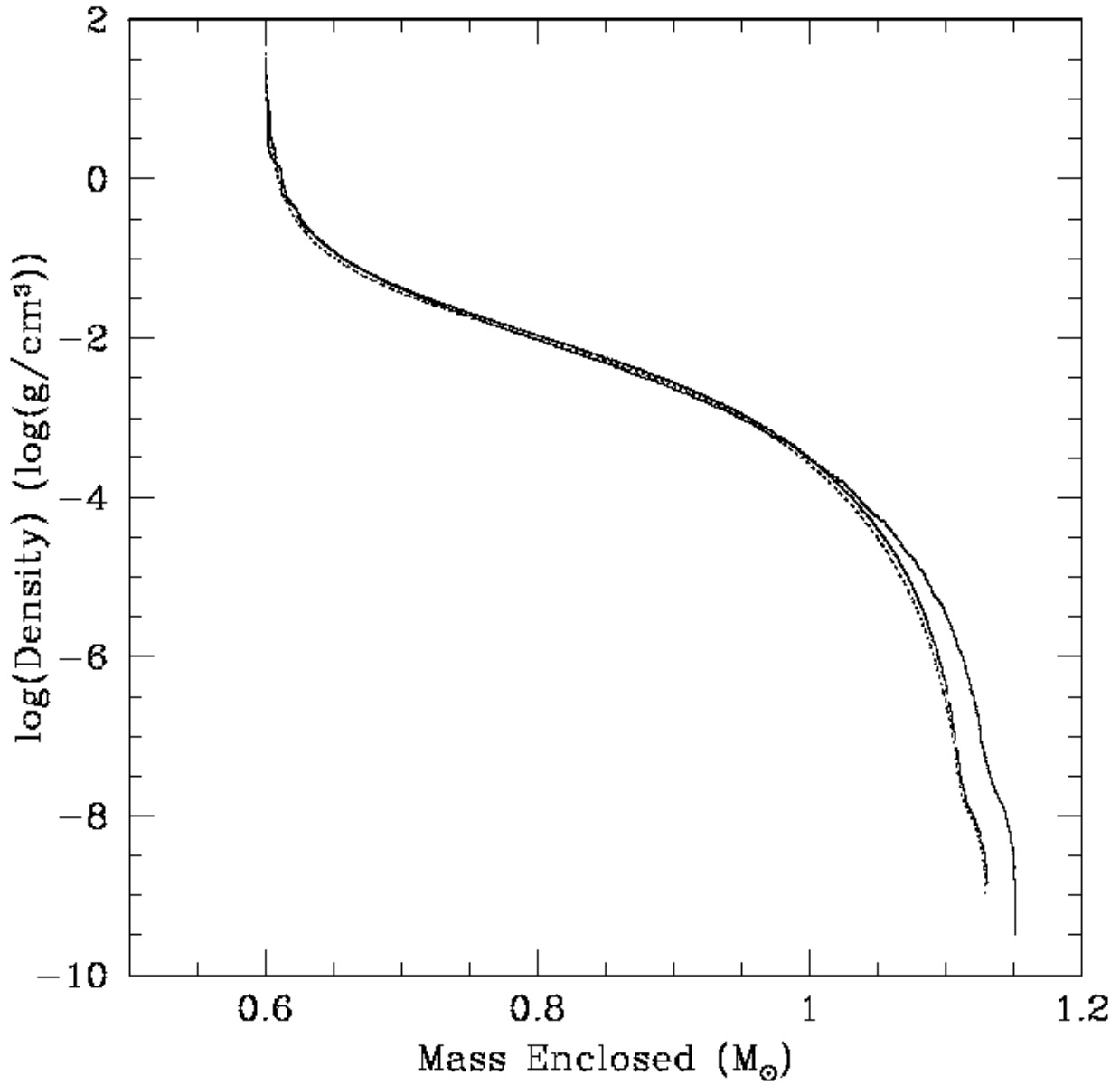


Fig. 3.— Logarithm of the density versus mass enclosed by an isodensity surface for the product of run AC with three different resolutions. The solid line is the product of a pre-main sequence star with  $\sim 10\,000$  particles, the long dashed line had  $\sim 50\,000$  particles in the parent PMS star, and the dotted line is the result of the same run with a  $\sim 100\,000$  particles PMS star.

noticeable differences between the 10 000 and 50 000 particle resolutions, the 50 000 and 100 000 resolutions are essentially indistinguishable. This indicates that the resolution we used in our simulations (10 000) was an adequate approximation since the daughter stars converge, as the number of particles is increased, to a model very similar to the one we achieved. Increasing the resolution simply further refined the results, not drastically altered them. As a result of this test, we concluded that while a resolution of 50 000 particles per parent star is optimal for an accurate description of the structure of the collision product (in agreement with Sills et al. (2002)), a lower resolution of 10 000 particles is sufficient to determine the product’s general properties.

### 3.2. A Representative Case

As a representative case, we will describe run C in detail. This is a collision between two PMS stars with an impact parameter of 1, and a relative velocity at infinity of 10 km/s. This collision took approximately 250 CPU hours to simulate. Figures 4-5 show the dynamical evolution through density contours at different stages of the collision. Despite the fact that the parameters predict that the collision would be just grazing, tidal effects caused the stars to be misshapen on approach and hence significant contact is made during the first pass. The stars go through 5 periastron passages before merging at a time of 730 hours. The collision product is rotating quickly, and is flattened by rotation, as seen in the x-z plane shown in figure 5b. There is an extended halo of material around the star, but it is not sufficiently flattened to be called a disk. The bulk of the material is within a radius of about  $7 R_{\odot}$ . This is significantly larger than the radius of a typical  $1.6 M_{\odot}$  main sequence star, but is comparable to a radius of a  $1.6 M_{\odot}$  pre-main sequence star on the Hayashi track. We expect that when this collision product contracts to the main sequence, it will be reasonably indistinguishable from a normal main sequence star.

Figure 6 shows the angular velocity as a function of cylindrical radius, the distance in the orbital plane to the rotation axis, of the daughter star of run C. This angular velocity data is only shown for particles within 2 smoothing lengths of the equatorial plane. This figure shows that the central region of the star is rotating at a constant rate. At a radius of about  $5 R_{\odot}$  the rotational velocity begins to drop and reaches a minimum at the edge of the star.

Figure 7 displays the density profile and figure 8 shows the entropy profile of the resulting star. Ideally, the entropy profile will be such that as you look at larger enclosed masses, the entropy always increases (ignoring the extreme edge of the star). This would imply that the inner majority of the star is in hydrostatic equilibrium (Lombardi, Rasio & Shapiro

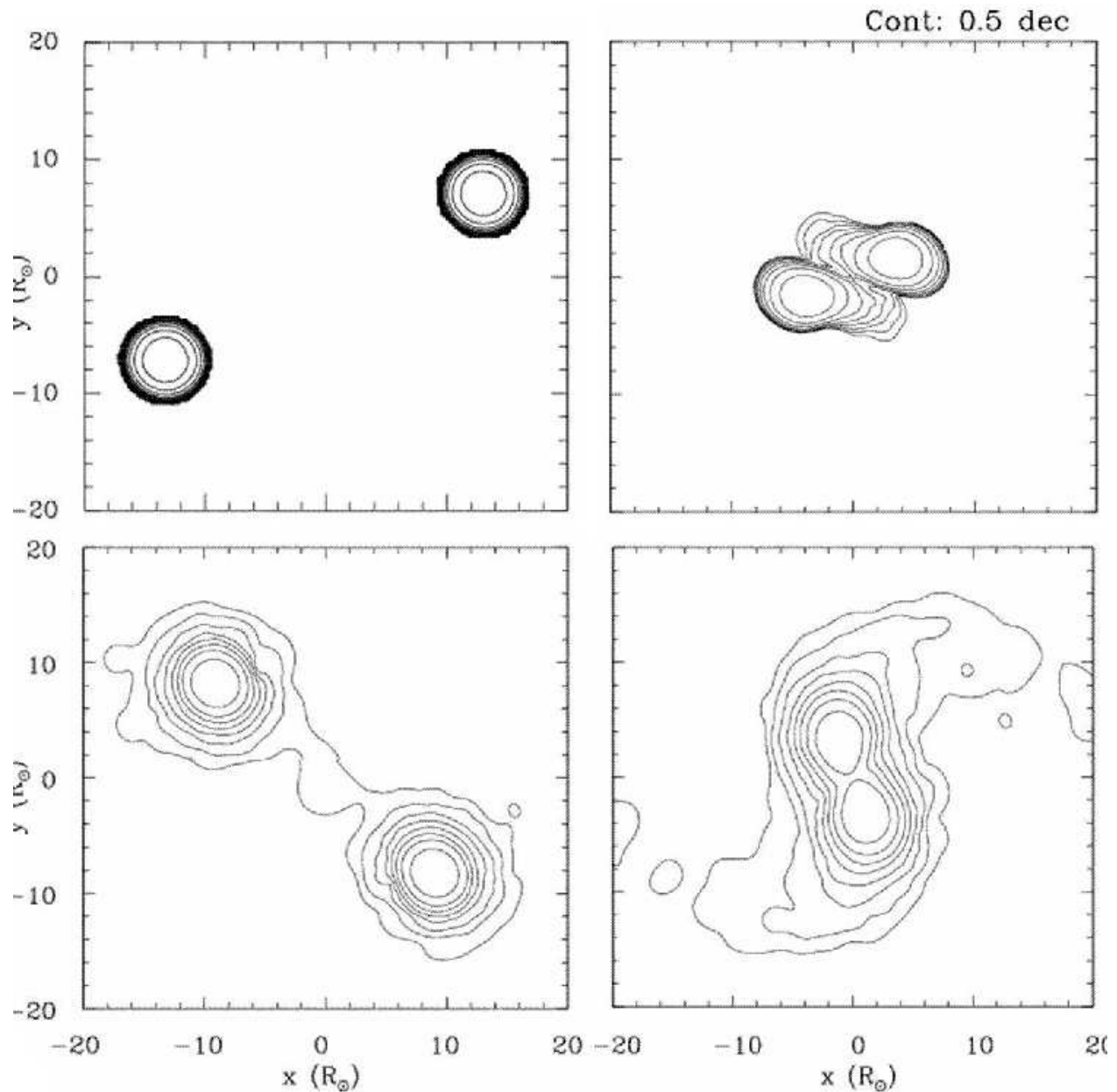


Fig. 4.— Density contours in the orbital plane spaced logarithmically from several stages of collision C. There are eight contours equally spaced over four decades down from the maximum density. The top left plot is at  $t=0$  hours, the top right is at 39 hours, the bottom left is at 542 hours, and the bottom right is at 690 hours.

Table 1. Table of Star Parameters

Star Name	Star Type	Mass $M_{\odot}$	Radius $R_{\odot}$	Number of SPH particles 1000's
PMS1	Pre-main Sequence	0.8	3.4	10
PMS2	Pre-main Sequence	0.8	3.4	50
PMS3	Pre-main Sequence	0.8	3.4	100
ZAMS	Zero Age Main Sequence	0.8	0.72	10
TAMS	Terminal Age Main Sequence	0.8	1.03	10
GB	Giant Branch	0.8	7.01	50
WD	White Dwarf	0.6	0.001	0

Note. — The giant branch star contains a point mass core of approximately  $0.22 M_{\odot}$  and  $0.028 R_{\odot}$ . The SPH particles model the remaining mass. Also, the white dwarf is modeled as a point mass.

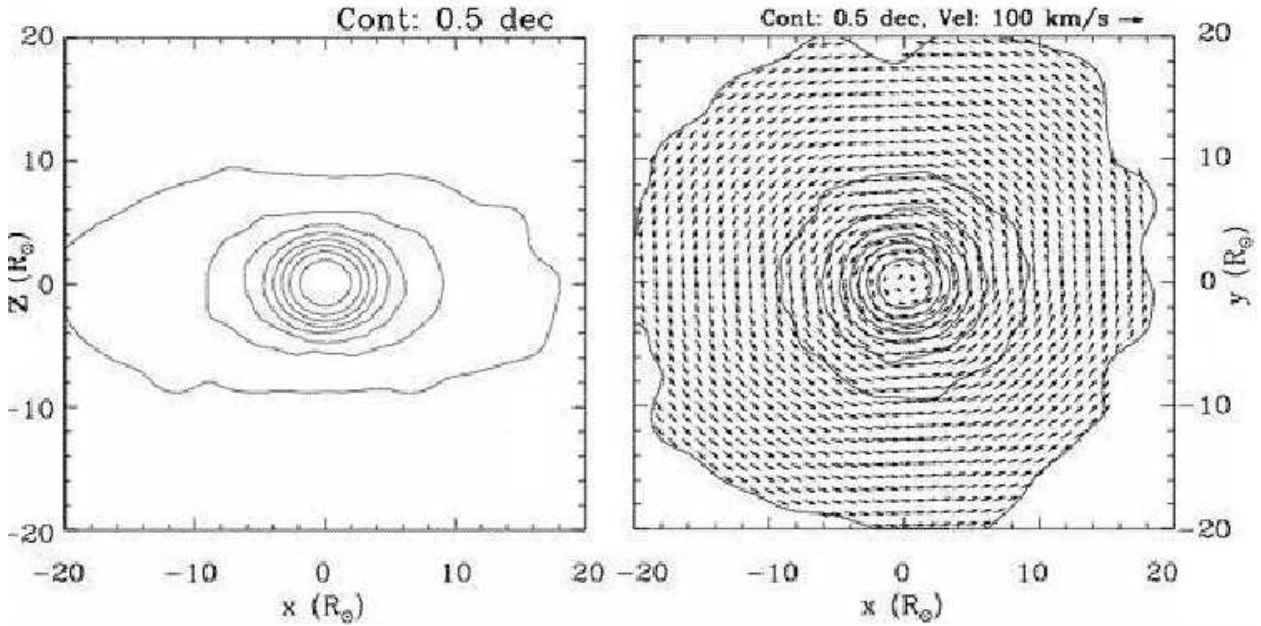


Fig. 5.— Density contours in the xz plane, spaced logarithmically, and velocity field in the orbital plane for the final product of collision C. Both plots are at the end time of the simulation:  $t=1767$  hours after the simulation began.

Table 2. Table of Run Results

Case	Impactor	$(\frac{r_p}{R_1+R_2})$	$(v_{inf})$ km/s	Merged	$M_{final}$ $M_{\odot}$	$J_{final}$ $g \frac{cm^2}{s}$	$\frac{T}{ W }$	Energy Conservation
A	PMS1	0.0	10	Y	1.55	6.77E48	1.47E-06	5.31E-3%
B	PMS1	0.5	10	Y	1.60	7.92E51	1.49E-2	6.69E-1%
C	PMS1	1.0	10	Y	1.60	1.12E52	3.53E-2	8.44E-1%
D	PMS1	0.0	40	Y	1.55	4.23E48	1.65E-6	3.16E-2%
E	PMS1	0.5	40	Y	1.59	7.92E51	1.31E-2	5.94E-1%
F	PMS1	1.0	40	Y	1.60	1.12E52	4.23E-2	7.89E-1%
G	PMS1	0.0	100	Y	1.54	3.97E48	2.12E-6	9.31E-2%
H	PMS1	0.5	100	Y	1.58	7.98E51	1.50E-2	6.18E-1%
I	PMS1	1.0	100	N	-	-	-	7.79E-1%
J	ZAMS	0.0	100	Y	1.47	7.81e+49	-1.09E-5	8.28E-1%
K	ZAMS	0.5	100	Y	1.48	2.02e+51	-7.59E-4	8.34E-2%
L	TAMS	0.0	10	Y	1.45	3.36E50	1.29E-5	4.31%
M	TAMS	0.5	10	Y	1.51	5.97E51	1.95E-3	4.15E-1%
N	TAMS	0.0	40	Y	1.44	2.53E50	9.86E-6	1.47%
O	TAMS	0.5	40	Y	1.51	5.86E51	1.99E-3	3.29E-1%
P	TAMS	0.0	100	Y	1.43	3.18E50	8.58E-6	8.62E-1%
Q	TAMS	0.5	100	Y	1.49	5.61E51	2.00E-3	1.92%
R	GB	0.0	10	Y	1.40	3.28E49	1.57E-5	1.00%
S	GB	0.5	10	Y	1.54	8.95E51	1.59E-2	4.60E-1%
T	GB	0.0	40	Y	1.40	2.23E49	1.47E-5	4.13E-1%
U	GB	0.5	40	Y	1.53	8.89E51	1.67E-2	5.40E-1%
V	GB	0.0	100	Y	1.38	1.76E49	1.60E-5	7.39E-2%
W	WD	0.0	10	Y	1.16	6.65E49	1.69E-5	9.10%
X	WD	0.5	10	Y	1.29	3.47E51	9.67E-3	12.9%
Y	WD	1.0	10	Y	1.28	4.72E51	1.38E-2	13.6%
Z	WD	0.0	40	Y	1.16	3.82E49	1.66E-5	14.1%
AA	WD	0.5	40	Y	1.29	3.52E51	1.01E-2	12.8%
AB	WD	1.0	40	Y	1.30	5.07E51	1.56E-2	10.1%
AC	WD	0.0	100	Y	1.15	5.56E49	1.70E-5	11.8%
AD	WD	0.5	100	Y	1.29	3.66E51	1.06E-2	12.7%
AE	WD	1.0	100	Y	1.27	4.96E51	1.58E-2	10.4%

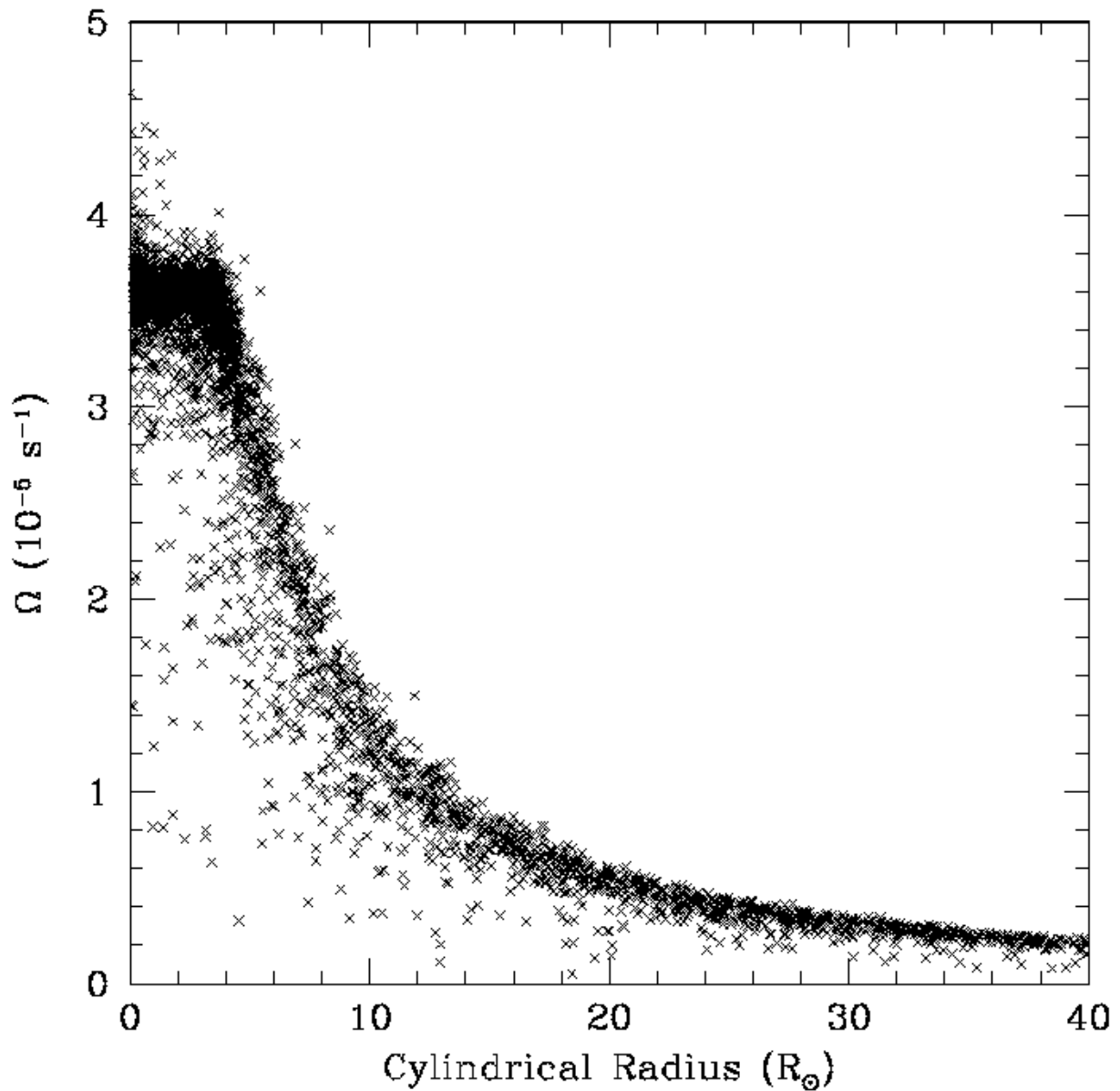


Fig. 6.— Angular velocity as a function of cylindrical radius for the final product of collision C.

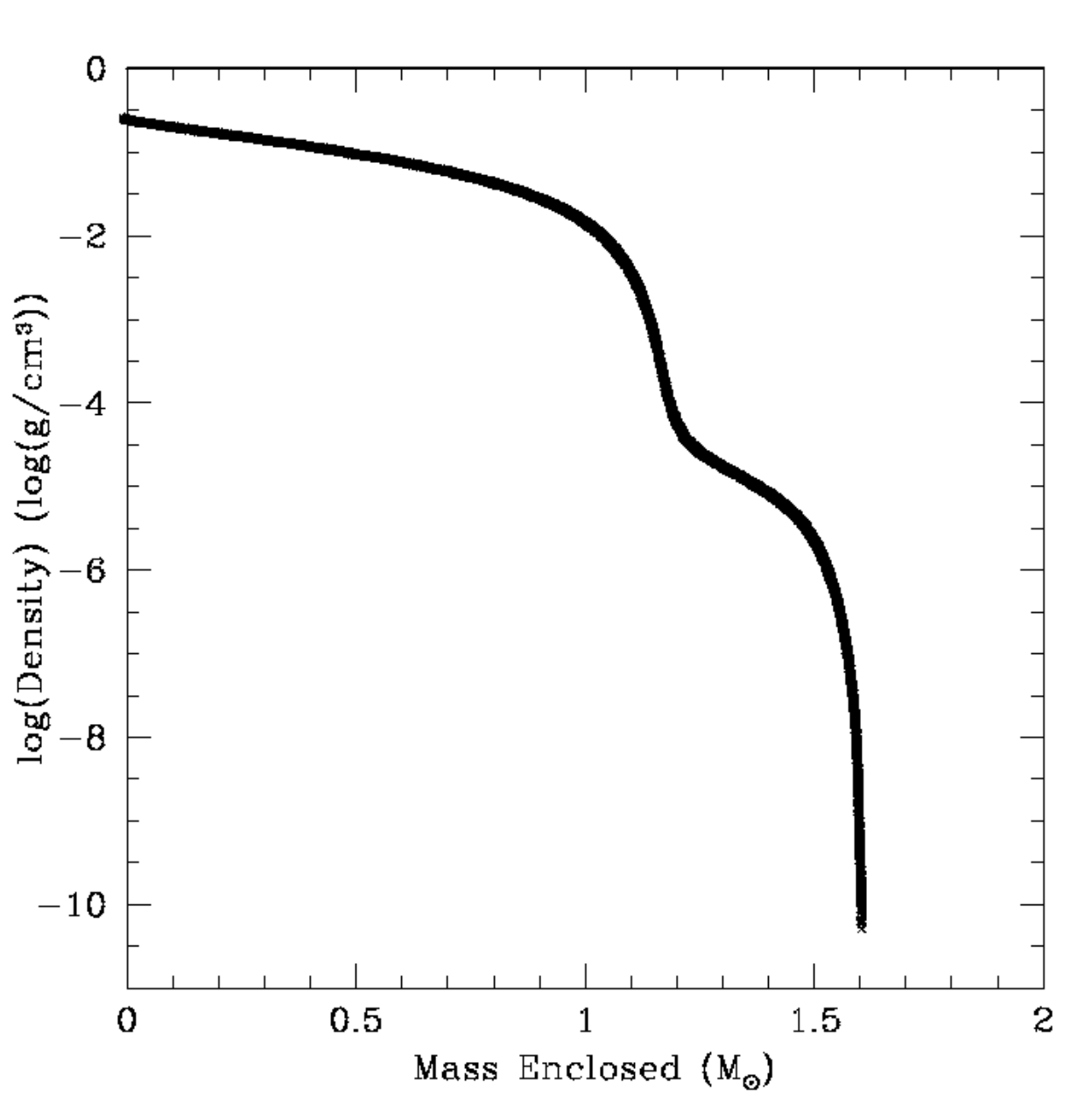


Fig. 7.— Density as a function of mass enclosed by isodensity surfaces for the final product of collision C.

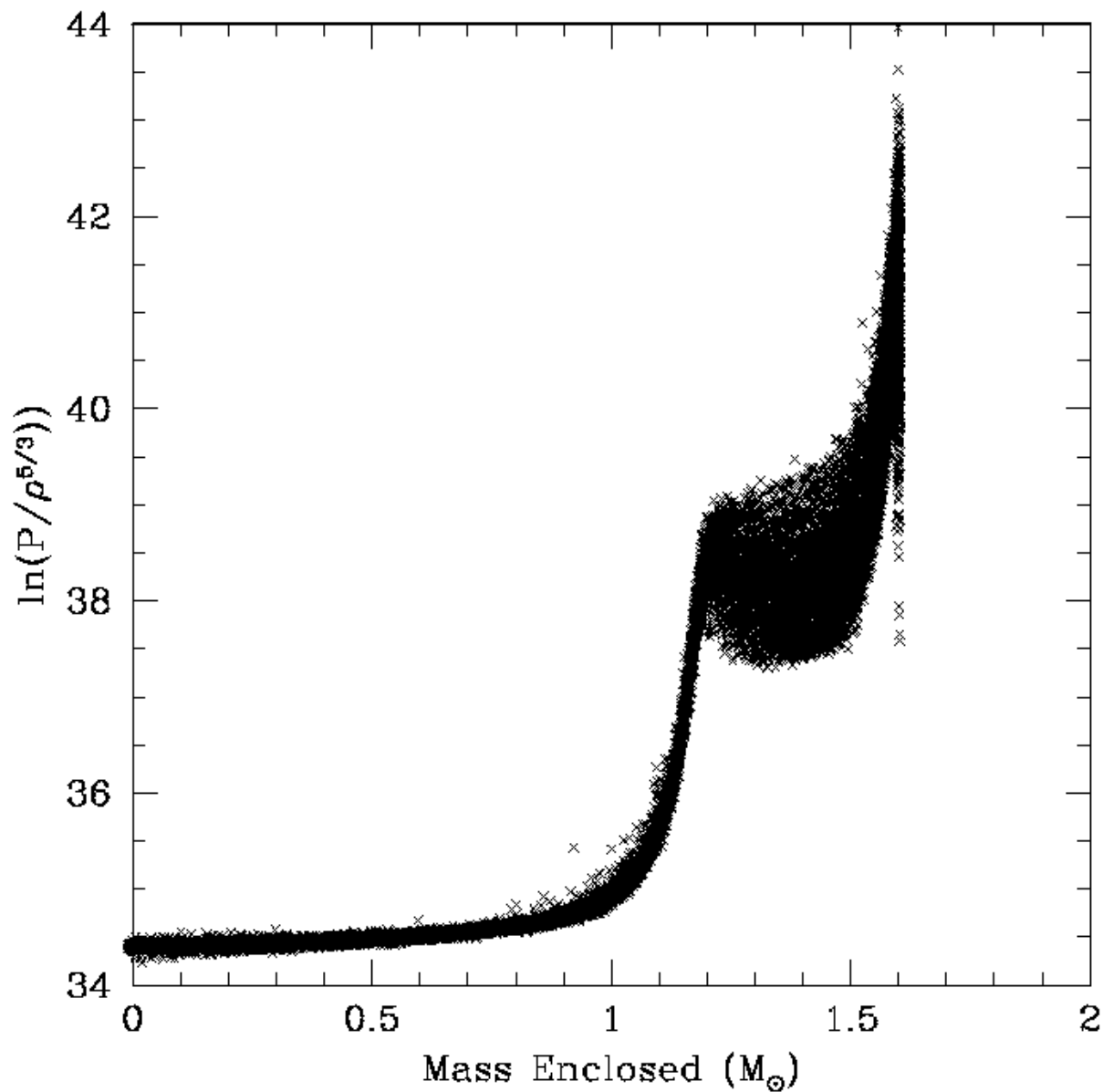


Fig. 8.— Entropy as a function of mass enclosed by isodensity surfaces for the final product of collision C. Pressure and density are measured in cgs units.

1996). Initially after the collision this is not the case; the entropy versus mass plots are very disordered. As the star relaxes, the inner region of the star begins to develop a well defined entropy curve. The region that is in hydrostatic equilibrium grows from the centre outward until this well defined curve extends essentially all the way to the edge of the star. However, we do not continue our simulations until the entire star is in hydrostatic equilibrium – the computational requirements are too large and we would be introducing unacceptably large errors in the total energy if we continued the simulation for the many more dynamical times required to bring the entire star into equilibrium. These simulations are sufficient to describe the behaviour of the inner 70% by mass of the daughter star.

In figure 9 the escaping mass as a function of time for run C is displayed. Each jump in the escaping mass represents a point of closest approach of the two stars. By the 4th pass the two stars are essentially merged into one. In this collision, only 0.5% of the total mass is lost from the system.

The energy plots for this collision followed a pattern typical to all cases studied. The energy as a function of time can be seen in figure 10. Total energy was conserved in this run to better than 1%. The internal, potential and kinetic energies fluctuated as the collision proceeded. The dips in potential energy and internal energy, which were mirrored by jumps in kinetic energy, correspond to points of closest approach of the two orbiting stars. As the stars moved towards their first closest approach point, potential energy was converted to kinetic energy, as the two stars sped up. At the moment of impact, energy is converted to internal energy, as a result of shock heating, at the expense of kinetic energy which is lost during the collision. As the two stars pass each other and begin to separate, the reverse process occurs with the potential increasing as the kinetic decreases. Each point of closest approach leads to another cycle of this process, with each time the minimum potential energy increasing and the maximum kinetic energy decreasing as the stars spiral into each other. After the third maximum in potential energy, the peaks in potential energy begin to decrease indicating that the stars are orbiting in a common envelope of material. Once the spikes have disappeared, the star has finally completed merging. Over the long run, as the star settles down, the kinetic energy was slowly lost to internal energy.

### 3.3. Results of the Other Simulations

The other runs give results similar to the run described above, with obvious differences dictated by the differences in impactor.

The only collisions which produced a star with a non-constant helium composition profile

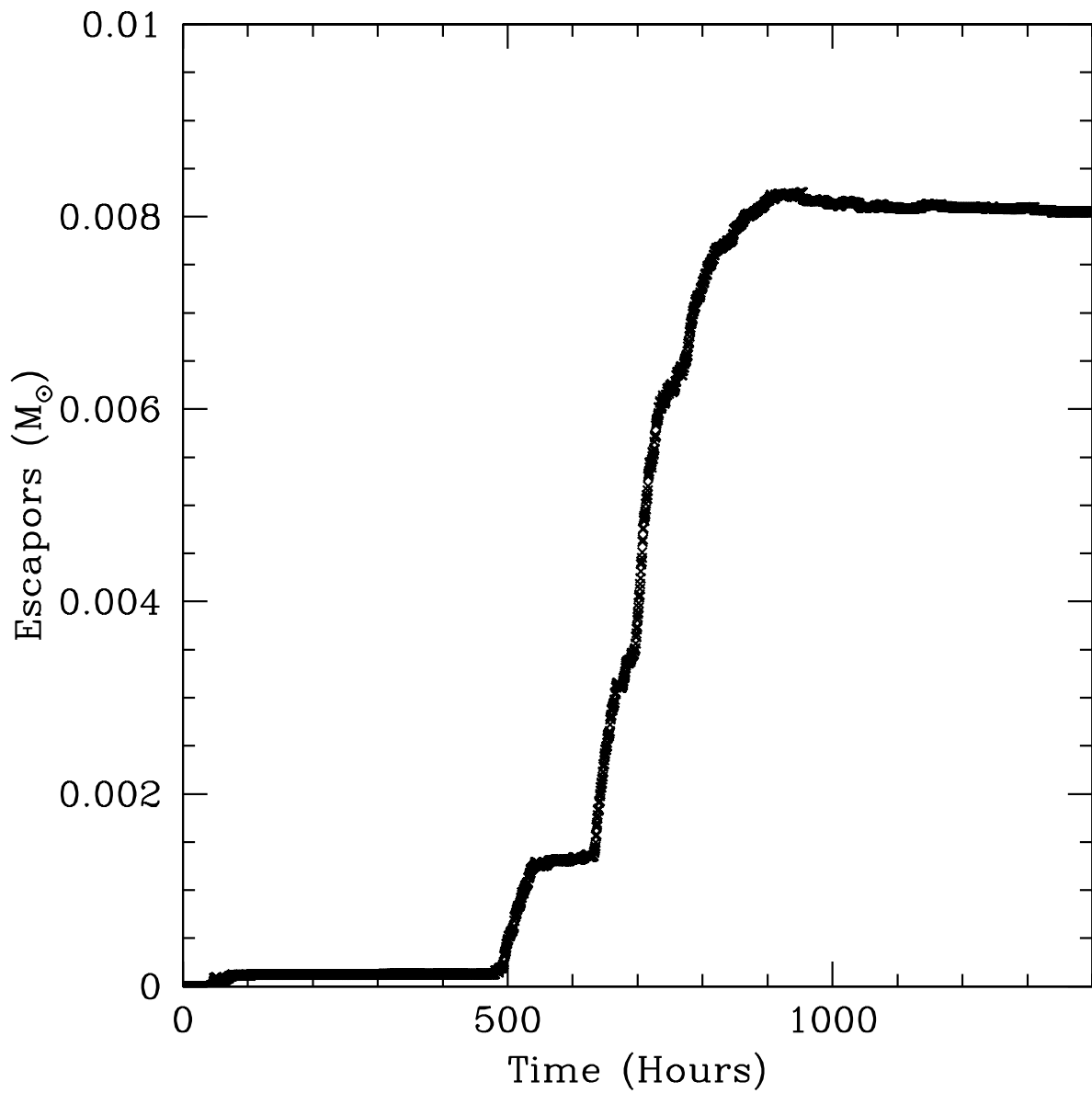


Fig. 9.— Escaped mass as a function of time for collision C.

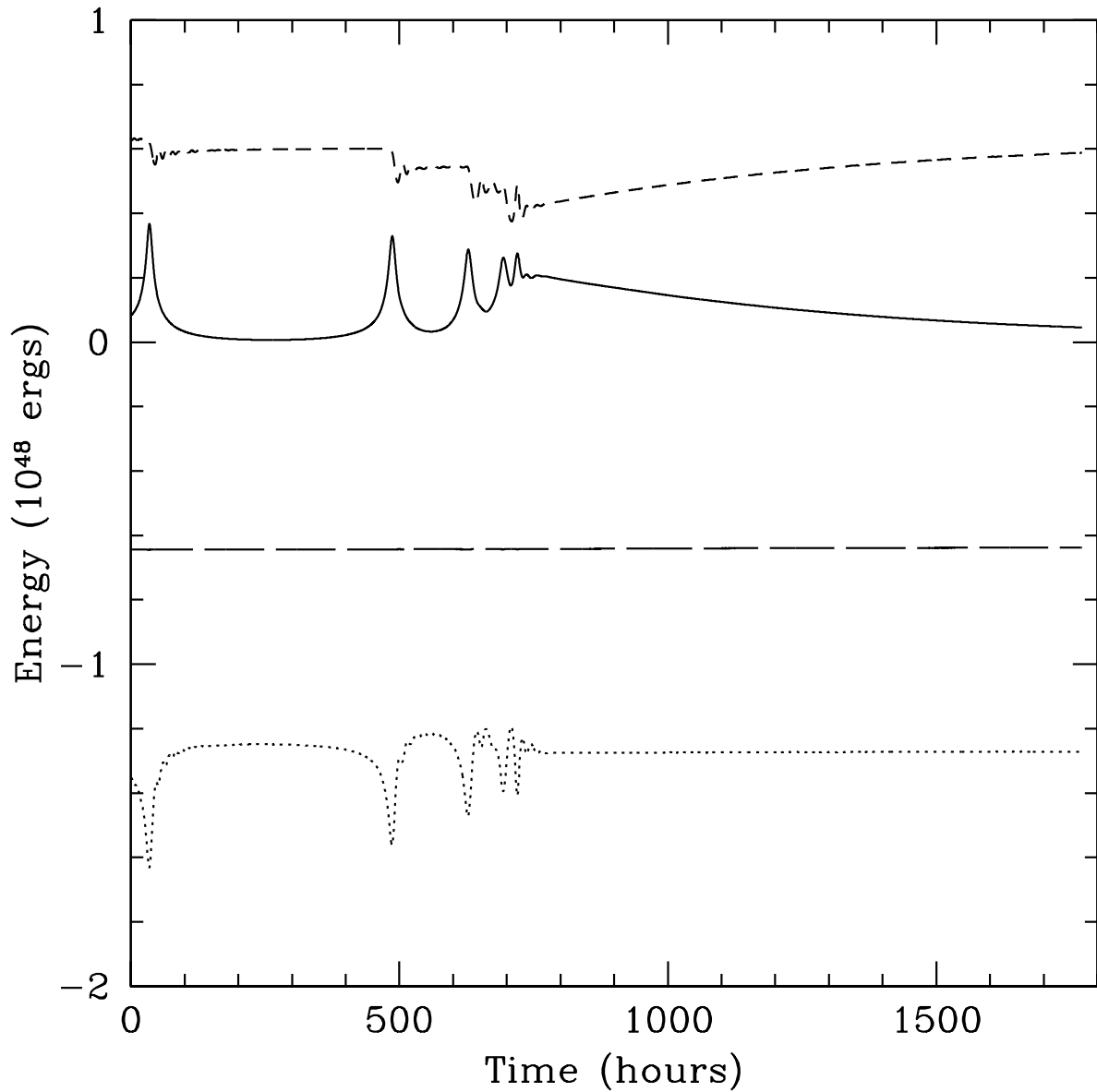


Fig. 10.— Energies as a function of time for collision C. The dotted line is the potential energy, the solid line is the kinetic energy, the long dashed line is the total energy, and the short dash line is the internal energy.

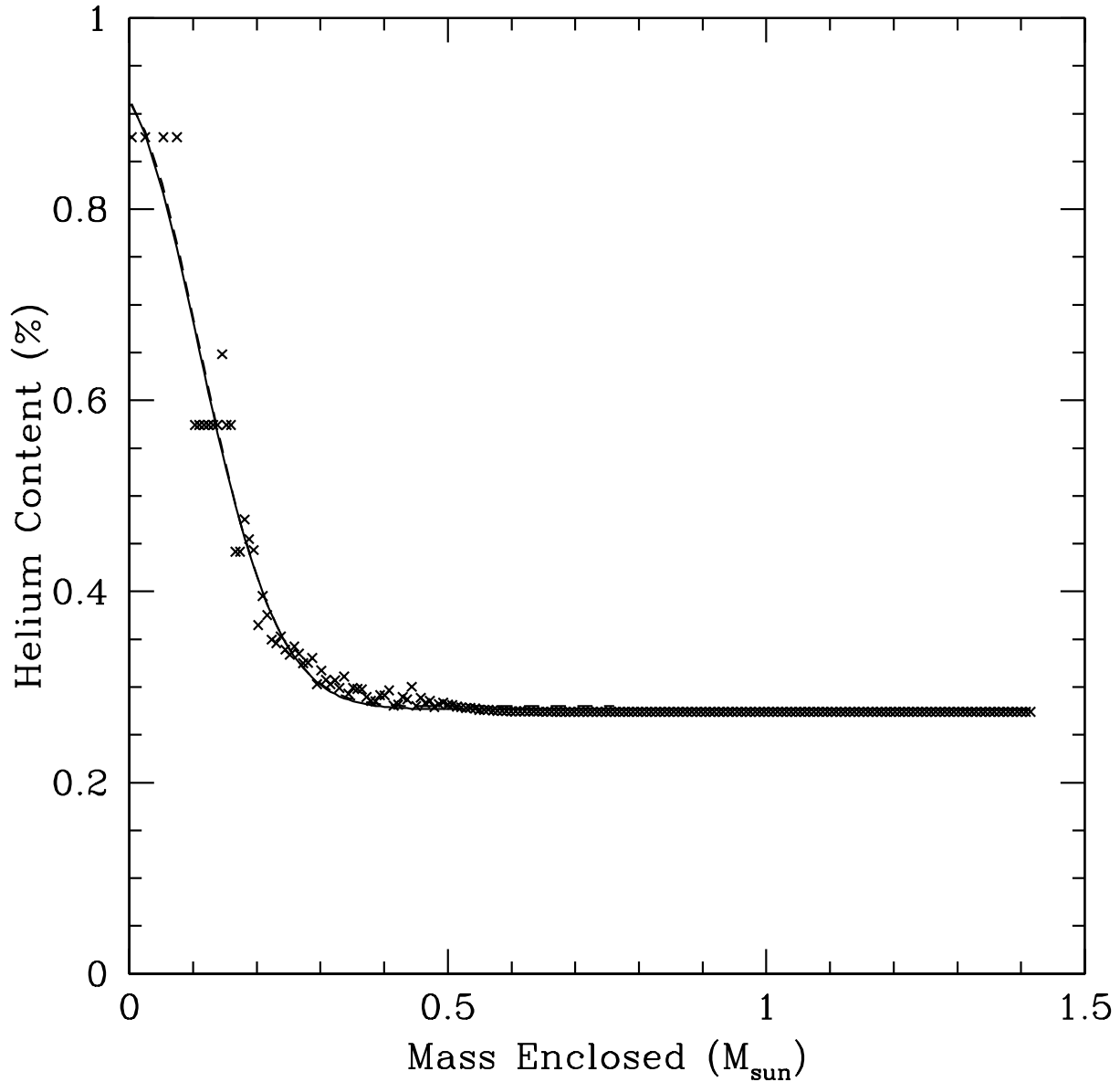


Fig. 11.— The helium composition as a function of enclosed mass for the collision product of run P. The x's are the average helium composition values for bins of specific radii and the solid line is a curve fitted to this data. The dashed line is the helium composition profile for the parent TAMS star.

were those between the TAMS and PMS star, due to the fact that the TAMS star was the only parent star with a varying helium composition profile. Figure 11 shows a plot of the helium composition for the result of run P. This was calculated by averaging the helium composition over annuli centered at the center of the daughter star. This plot shows that the overall shape of the profile remains approximately the same as the original TAMS star.

Figure 12 shows the density profiles of collision products of head-on collisions (with  $v=100\text{km/s}$ ) between pre-main sequence stars and other objects. In this figure, only the SPH particles have been included. Some simulations include a point mass (e.g. the white dwarf and the core of the giant). Those collision products have density profiles which start at masses greater than zero, with the point mass taking up the inner regions.

These density profiles, combined with the composition information we have for these collision products, hint at what the subsequent evolution of these stars will be. There are some interesting trends to notice. First, the central density of the collision product depends on the central density of the impactor, in that the more evolved impactors produce more centrally concentrated collision products. This is in agreement with trends suggested by earlier simulations of collision products (Lombardi, Rasio & Shapiro 1996). More evolved stars have higher central densities and therefore lower central specific entropies. Gentle stellar collisions can be modeled by entropy-sorting of the fluid from both stars, and so the cores of evolved stars will end up at the centre of any collision product. The more evolved a star is, the more of it will have low entropy and will move to the core of the daughter star.

Another interesting trend is that the total mass of the collision product is lower as the impactor gets more evolved. The PMS+GB collision has a total mass of  $1.38 M_{\odot}$ , while the PMS+PMS collision product has a mass of  $1.55 M_{\odot}$ . The larger mass loss with more evolved (and hence more compact) impactors is related to the amount of shock-heating in the collision. The PMS+WD collision product actually loses a smaller percentage of its total mass than the PMS+GB collision since the white dwarf as we model it does not have an atmosphere to be shock heated during a collision. Therefore, all the mass lost during the collision must come only from the pre-main sequence star.

A goal of this paper is to predict the evolutionary state of the collision products after the collision, and these density profiles will help us do that. First, the PMS+PMS collision results in a very extended, fluffy object with no composition gradient. This object will return to the pre-main sequence phase on a thermal timescale, and will simply be a more massive PMS star. It will be indistinguishable from other stars of the same mass, except that it will be (slightly) delayed in its evolution. However, the difference in age between a  $1.5 M_{\odot}$  collision product and a normal  $1.5 M_{\odot}$  star in the same cluster will be at most a few 10's of Myr, and probably not observable except under exceptional circumstances.

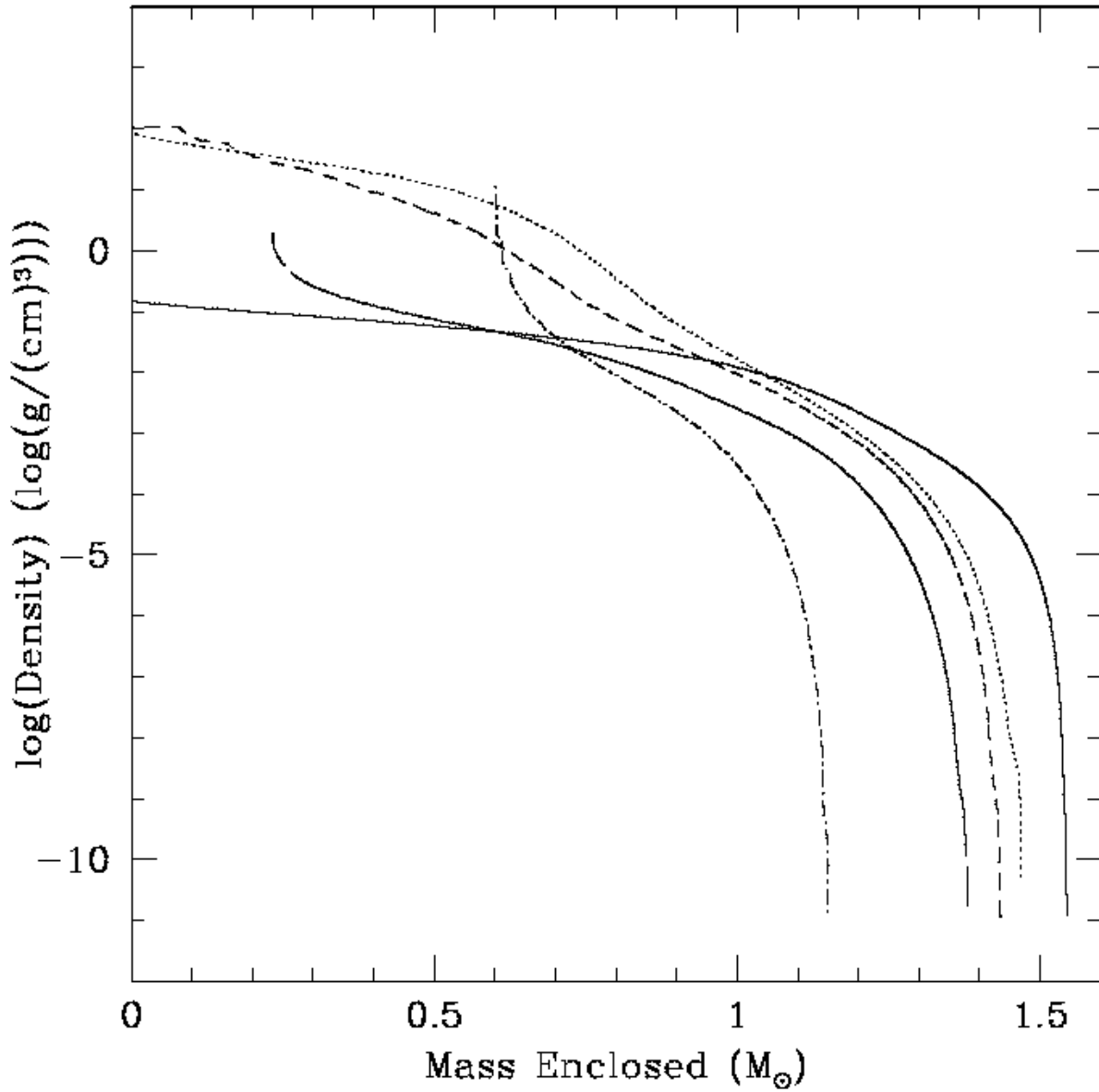


Fig. 12.— Density as a function of mass enclosed for collisions G (PMS+PMS, solid line), J (PMS+ZAMS, dotted), P (PMS+TAMS, short dash), V (PMS+GB, long dash), and AC (PMS+WD, dash-dot).

The two PMS+MS collision products have denser cores than the PMS+PMS collision product, and a steeper density gradient. These stars will relax to become main sequence stars. As we can see from figure 11, some hydrogen-rich material has been mixed into the core of the PMS+TAMS collision product, but not very much. Therefore, these collision products can be well-modeled as ‘rejuvenated’ stars – their evolution will be the same as that of a normal star of their mass, but the starting point of these collision products is determined by the helium content of their cores. If the main sequence impactor was near the end of its main sequence life, then the collision product will be near the end of its life.

Both the PMS+WD and PMS+GB collision products have ‘point masses’ at their core. These point masses, which are very dense, and probably degenerate, come from either the initial giant or the entire white dwarf. Therefore, the collision product will look very much like a giant star – a dense core surrounded by a hydrogen-rich envelope. Again, the evolutionary starting point of the collision product will be determined by the impactor. The core mass of the new giant will be given by the core mass of the initial giant, or by the mass of the white dwarf. In some cases, the evolution will be a little odd – for example, the core mass of our PMS+WD collision product is  $0.6 M_{\odot}$ , much larger than the canonical  $0.45 M_{\odot}$  required for helium core flash in low mass stars. That collision product will probably evolve rapidly to the horizontal branch stage, resulting in an unusually massive HB star. Collisions between PMS and giants, however, will result in massive giants with reasonably small core masses. They will be slightly bluer than normal giant branch stars in the cluster, and will also produce unusually bright and red horizontal branch stars when they reach that stage. These could be one explanation for the supra-horizontal branch stars seen in some globular clusters (Bailyn 1994; Ferraro et al. 1999), for example (although we do not expect that this is the dominant mechanism as the relevant timescales are quite short).

For a given impactor, the amount of mass lost by the system increases as the impact parameter decreases. The more grazing the collision, the less likely particles are to be given a radial velocity sufficient to free them from the stars gravitational bound, and thus the escaper mass is less. However, the mass lost is almost independent of velocity at infinity. The velocity of the encounter seems to have little effect on the mass lost during the collision. The mass lost only increases slightly for higher velocity collisions. All collisions, even the most gentle, result in impact speeds which are larger than the sound speed in the outer layers of the PMS star. All the gas that could easily be shock-heated, has been heated, and has been lost. As expected, the total angular momentum of the system is larger for larger impact parameters, since the angular momentum comes only from the initial orbit.

We expect that these results are basically independent of the mass of the pre-main sequence star. The structure of these low mass stars is quite similar. Since they are chemically

homogeneous and fully convective, pre-main sequence stars have almost constant entropy throughout their interior. Since they are larger and less dense, they have more entropy than a main sequence star of the same mass. Gentle stellar collisions result in a 'sorting by entropy' of the two parent stars (Lombardi et al. 2002). Our result that the pre-main sequence star forms an envelope around any more evolved star during a collision is in agreement with this general picture, and should be independent of the masses of the pre-main sequence stars involved.

It seems clear from our simulations that dynamical models of clusters do not need to include detailed (hydrodynamic) models of collision products that involve pre-main sequence stars. A simple prescription based on the structure of the impactor and assuming a mass loss of a few percent of the total mass should suffice for most dynamical simulations at the moment. Since pre-main sequence stars are chemically homogeneous, they are even simpler to model than main sequence stars. Current dynamical simulations of clusters that include the effects of stellar collisions (e.g. Hurley et al. 2001; Portegies Zwart et al. 2001) use a formulaic prescription for the rejuvenation of main sequence stars when they collide with each other; such a prescription could be easily modified to include the effects of pre-main sequence stars. Efforts to include full stellar evolution codes into stellar dynamics codes are in their infancy, but are being spearheaded by the MODEST collaboration (Hut et al. 2003).

#### 4. Summary

We have performed simulations of collisions between pre-main sequence stars and a variety of other kinds of stars. We investigated the effects of impact parameter and velocity of encounter, with the goal of determining the structure and likely evolution of the collision products. We find that pre-main sequence stars are not very disrupted by collisions, and tend to wrap themselves around the outside of their impactors. As the impactor becomes more evolved (and hence more dense), the pre-main sequence star material gains more energy in the collisions and is less likely to remain bound to the system. The mass lost by the collision increases as the impact parameter decreases, and is largely independent of the velocity of the encounter in the range we studied ( $v_{\text{inf}} = 10 - 100 \text{ km s}^{-1}$ ).

The subsequent evolution of the collision products was speculated based on their density and composition profiles immediately after the collision. PMS+PMS collision products should become higher mass pre-main sequence stars. PMS+MS collisions should produce higher mass main sequence stars with their starting point on the evolutionary track determined by the helium content of the main sequence impactor's core. Collisions between pre-main sequence stars and stars with helium cores or white dwarfs should result in gi-

ant branch stars, with their initial evolutionary point determined by the core mass of the impactor.

DL is supported in part by an NSERC Undergraduate Summer Research Award. AS is supported by NSERC. The simulations reported in this paper were performed at the SHARCNet facilities at McMaster University.

## REFERENCES

Aarseth, S. J. 1996, IAU Symp. 174: Dynamical Evolution of Star Clusters: Confrontation of Theory and Observations, 174, 161

Bailyn, C. D. 1994, AJ, 107, 1073

Bate, M.R., Bonnell, I.A., Price, N.M., 1995, MNRAS, 277, 362

Benz, W., 1990, in Buchler J. R., ed., The Numerical Modeling of Nonlinear Stellar Pulsations: Problems and Prospects. Kluwer, Dordrecht, p. 269

Cohn, H. 1980, ApJ, 242, 765

Elson, R., Hut, P., & Inagaki, S. 1987, ARA&A, 25, 565

Ferraro, F. R., Paltrinieri, B., Rood, R. T., & Dorman, B. 1999, ApJ, 522, 983

Guenther, D. B., Demarque, P., Kim, Y.-C., & Pinsonneault, M. H. 1992, ApJ, 387, 372

Hurley, J. R., Tout, C. A., Aarseth, S. J., & Pols, O. R. 2001, MNRAS, 323, 630

Hut, P., & Inagaki, S. 1985, ApJ, 298, 502

Hut, P., et al. 1992, PASP, 104, 981

Hut, P., et al. 2003, New Astronomy, 8, 337

Lombardi, J. C. Jr., Rasio, F. A., Shapiro, S. L. 1996, ApJ, 468, 797

Lombardi, J. C., Warren, J. S., Rasio, F. A., Sills, A., & Warren, A. R. 2002, ApJ, 568, 939

Monaghan, J.J, 1992, ARA&A, 30, 543

Portegies Zwart, S. F., McMillan, S. L. W., Hut, P., & Makino, J. 2001, MNRAS, 321, 199

Siess, L., Dufour, E., & Forestini, M. 2000, A&A, 358, 593

Sills, A., Lombardi, J. C., Jr., 1997, ApJL, 484, 51

Sills, A., Lombardi, J. C., Bailyn, C. D., Demarque, P., Rasio, F. A., & Shapiro, S. L. 1997, ApJ, 487, 290

Sills, A., Adams, T., Davies, M. B., Bate, M. R. 2002, MNRAS, 332, 49